Rate constants and branching ratios for the reactions of various positive ions with naphthalene from 300 to 1400 K

Anthony J. Midey, Skip Williams, Susan T. Arnold[1], Itzhak Dotan[2],
Robert A. Morris, A.A. Viggiano*

Air Force Research Laboratory, Space Vehicles Directorate, 29 Randolph Road, Hanscom Air Force Base, MA 01731-3010, USA

Abstract

Temperature dependent rate constants and branching ratios are reported for the reactions of a variety of ions with recombination energies ranging from 9.26 eV (NO^+) to 21.56 eV (Ne^+) with naphthalene. For most ions, the measurements are made between 300 and 370 K in a variable temperature-selected ion flow tube (VT-SIFT). For the reactions of Ar^+ and N_2^+, data have also been measured between 300 and 500 K in the selected ion flow tube. In addition, for the reactions of O_2^+ and N_2^+, data have been obtained between 500 and 1400 K in a high temperature flowing afterglow (HTFA). These are among the first determinations of branching ratios for ion–molecule reactions measured over 700 K. All reactions are found to proceed at the Langevin collision rate for all temperatures studied. The reactions proceed by nondissociative and dissociative charge transfer except for the reaction involving F^+ where some of the reactivity is attributed to chemical channels. No dissociative charge transfer is observed for ions with recombination energies equal to or less than that for N_2^+ at room temperature. At higher temperatures in the N_2^+ reaction and for ions with higher recombination energies (F^+, Ne^+), naphthalene cation dissociation is observed, implying a threshold over 16 eV. This value is substantially higher than the known thermodynamic threshold because of kinetic shifts and quenching of the excited state of $C_{10}H_8^+$ by collisions with the helium buffer gas. The observed product thresholds and branching ratios are presented within the context of previous work and the implications for combustion chemistry are discussed. (Int J Mass Spectrom 195/196 (2000) 327–339) © 2000 Elsevier Science B.V.

Keywords: Ion molecule; Rate constants; Kinetics; Naphthalene; High temperature; Combustion; Ion chemistry

1. Introduction

Polycyclic aromatic hydrocarbons (PAHs) play an important role in combustion chemistry. For example, pyrolysis of hydrocarbons produces carbonaceous de-posits through complex chemical reactions involving PAHs such as naphthalene. Furthermore, condensation reactions such as Diels–Alder additions generate increasingly larger ring compounds from neutral PAHs, promoting the formation of tars and soot [1]. Recently, soot formation via PAH growth has been modeled [2]. Although experiments have shown that PAH cations may also undergo successive ring additions, further contributing to soot formation [3,4], the effects of ion chemistry have not been included in the models.

We have begun investigating the effects of ioniza-

* Corresponding author. E-mail: viggiano@plh.af.mil

[1] Under contract to Aerodyne Research, Inc., Billerica, MA.

[2] NRC Senior Research Fellow. Permanent address: Department of Natural and Life Sciences, Open University of Israel, 16 Klausner St. Ramat-Aviv, Tel-Aviv, Israel.

Dedicated to Bob Squires for his many seminal contributions to mass spectrometry and ion chemistry.

tion on combustion processes. Previously, reactions of various atmospheric plasma ions (NO^+, N_2^+, O_2^+, O^+, N^+) with aliphatic hydrocarbons have been studied as a function of temperature using flow tube methods [5–7]. Incorporating these ionic mechanisms into detailed hydrocarbon combustion kinetics models demonstrates that ionization may speed the rate of combustion [8]. In order to expand the database of ion chemistry available for the combustion kinetics and soot formation models, we have undertaken a study of atmospheric plasma ions reacting with aromatic hydrocarbons.

In this article, we present temperature dependent rate constants and product branching ratios for the reaction of several air plasma ions (NO^+, N_2^+, N^+, O_2^+, O^+) with naphthalene. These reactions have been examined using a variable temperature-selected ion flow tube (VT-SIFT) from 300–500 K. A high temperature flowing afterglow (HTFA) allows the reactions of O_2^+ and N_2^+ to be further studied from 500–1400 K. These measurements, along with similar ones for reactions with benzene [9], are the first branching ratios measured in the HTFA and are therefore the first ion–molecule branching ratios measured at high temperatures. This advancement is noteworthy because branching ratios can now be measured at relevant combustion temperatures.

In addition to being important in combustion processes, PAHs have long been of interest because they are believed to exist in the interstellar medium in both neutral and cationic forms [10]. PAHs may account for a portion of the spectral features observed in space [11,12]; recent models using the spectral features of a mixture of neutral and cationic PAHs including naphthalene successfully reproduce many interstellar infrared emission features [13]. Under the conditions that exist in space, PAH cations may also undergo dissociation [14,15]. The dissociation of the naphthalene cation, $C_{10}H_8^+$, has been previously studied in other laboratories [14,16–28]. Briefly, the main product ions of $C_{10}H_8^+$ dissociation result from the elimination of H atoms and $C_{2n}H_2$ molecules [14,17–19,21,22,24,27,28]. The energetics of $C_{10}H_7^+$ and $C_8H_6^+$ product formation have been particularly well established [24]. Other dissociation product ions arise

at high energies, indicating that substantial fragmentation of the naphthalene cation occurs [19–21]. Comparing time-dependent dissociation measurements to Rice–Ramsperger–Kassel–Marcus (RRKM) calculations has provided valuable information on the $C_{10}H_8^+$ dissociation lifetime, which is surprisingly long [19,21,22,24].

In order to further explore the dissociation of $C_{10}H_8^+$, we have extended the current study of naphthalene reacting with atmospheric plasma cations to include several high energy ions as well, namely Ar^+, F^+, and Ne^+. Taken together, this set of cation reactions allows for comparison of the flow tube studies with the previous $C_{10}H_8^+$ dissociation studies. In addition, it allows us to explore the effects of electronic, vibrational, and rotational energy on the reactivity.

2. Experimental

Both the VT-SIFT [29] and the HTFA [30] have been described in detail elsewhere. The methods complement each other, providing the capability for studying reactions over temperatures ranging from 85–1800 K at pressures from 0.25–2 Torr. A brief description of the methods as applied to the current problem follows.

The VT-SIFT uses a differentially pumped high pressure electron impact ion source with a quadrupole mass spectrometer for mass selection. The desired reactant ion is injected into the flow tube where a fast flow of helium buffer gas entrains the ions and carries them into the reaction region where the naphthalene is introduced. The remaining reactant ions as well as all of the product ions are sampled through a small orifice and mass analyzed in a quadrupole mass spectrometer. Monitoring the depletion of the reactant ion over a previously measured reaction time as a function of the naphthalene concentration allows the reaction rate constant to be calculated under pseudo-first order conditions. The absolute error in the reported rate constants is $\pm 25\%$, whereas the relative error is $\pm 15\%$ [29].

Naphthalene enters the flow tube through a bubbler

system where helium carrier gas passes through a sample of naphthalene crystals, becoming saturated with naphthalene vapor. The flow rate of naphthalene is derived from the known vapor pressure of naphthalene at room temperature [31] along with the helium flow rate and the total pressure in the bubbler. Adjusting the helium flow varies the concentration of naphthalene introduced into the reaction region. The naphthalene flow rate is roughly proportional to the square root of the helium flow rate [32].

Rate constants in the HTFA are measured in a similar fashion as in the VT-SIFT, the key difference being the lack of ion selection in the HTFA. Penning ionization of the source gas by metastable He atoms as well as charge transfer with He^+, both created through electron impact, generate the reactant ions. A large flow of source gas must subsequently be added to guarantee that all of the metastables, He^+ ions, and any electronically excited reactant ions are consumed before the reaction zone. The presence of any of these species in the reaction zone can produce erroneous results. The rate constants have relative uncertainties of $\pm15\%$ and absolute uncertainties of $\pm25\%$ [30].

Primary ions of simple molecules can now be made with near 100% purity because more efficient pumping on the vacuum box surrounding the furnace and flow tube reduces the water vapor concentration in the flow tube. This improvement also permits product branching ratios to be measured for the first time in the HTFA. The branching ratios are determined in the following manner in both experiments. First, the product mass resolution is set low enough to minimize mass discrimination between the $C_nH_m^+$ products, where $n = 6$, 8, and 10 for the major product channels. The resolution is set low enough so that ions with the same number of carbons but varying numbers of hydrogens are detected as one unresolved peak. Extrapolating the product branching ratios to zero flow of naphthalene gives the partitioning of the products into the various C_n channels, regardless of any secondary chemistry that may occur. Next, the resolution is set high enough to resolve the 1 amu difference between the various $C_nH_m^+$ products for a given n. The branching ratios are measured again to determine how the intensity of the low-resolution C_n

mass peak is distributed amongst the different $C_nH_m^+$ products. A similar extrapolation to zero neutral reagent flow gives the relative high-resolution product fractions that are multiplied by the low-resolution fraction of the C_n peak to give the overall contribution of an individual product channel. This method has been successfully employed in similar branching ratio determinations with relative uncertainties of $\pm25\%$ [5].

The high-resolution product branching ratios are further corrected for the $^{13}C_nH_m^+$ contribution to the product peak at 1 amu higher mass. An additional correction has been made to the HTFA branching ratios for N_4^+ formed in the flow tube at temperatures below 1100 K in the N_2^+ experiments. The recombination energy of N_4^+ is about 12.9 eV [33], which is between the recombination energies of O_2^+ and O^+. The latter two ions only undergo nondissociative charge transfer; therefore, we assume that the N_4^+ signal in the HTFA contributes only to the $C_{10}H_8^+$ mass peak. The N_4^+ signal has consequently been subtracted from the $C_{10}H_m^+$ signal at low mass resolution, and the branching ratios have been renormalized to reflect the change. This correction is about 15% at 500 K and eventually becomes unnecessary at higher temperatures where N_4^+ is unstable. The relative uncertainty in the branching ratio determinations is $\pm30\%$.

Alkali metal atoms and ions emitted from the industrial-grade quartz flow tube at temperatures above 800 K do not interfere with the branching ratio measurements of naphthalene. However, monitoring the alkali ion signal during a kinetics experiment has proven to be a valuable diagnostic tool. If the alkali ion signal does not vary with neutral reagent concentration, then the complex flow tube chemistry has equilibrated before the reaction zone, and all unwanted species from the source region have been scavenged.

The reagent sample has been used without further purification except for pumping on the naphthalene sample to removed trapped gases. The naphthalene is of >99% purity (Aldrich, 99+%, scintillation grade) and the helium carrier gas is 99.997% pure (AGA). The buffer gas used in both flow tubes is helium of the

same grade and supplier. However, the helium buffer gas is passed through a liquid nitrogen cooled sieve trap to remove any water vapor. The nitrogen and oxygen source gases used to create N_2^+, O_2^+, O^+, and N^+ ions are 99.999% pure (AGA). Other source gases employed are argon (AGA, 99.999%), nitric oxide (Matheson, 99.3%), and neon (Matheson, 99.999%). Generating F^+ ions necessitates the use of sulfur hexafluoride (Matheson, 99.8%) as the source gas, requiring a rhenium filament in the source instead of the thoriated iridium filaments normally used.

3. Results

Temperature dependent rate constants and product branching ratios for the reactions of naphthalene with NO^+, O_2^+, O^+, N^+, N_2^+, Ar^+, F^+, and Ne^+ as measured in the VT-SIFT and HTFA are given in Tables 1 and 2, respectively. Reaction enthalpies at 298 K have been calculated for the observed products and are listed in Table 1. The standard heats of formation utilized in the calculations are from Lias et al. [34]. To calculate the energetics, we make assumptions about product structures based on the literature [14,19–22,24,26,35,36]. When previous data are not available, we assume that the lowest energy channel occurs. The neutral fragments generated are not observed in our experiment. In addition, several isomers of the ionic and neutral products may occur that have energies within 1 eV of each other [34]. In some cases, the neutral products are shown in parentheses to reflect this uncertainty. Enthalpies enclosed in braces indicate that estimates have been made regarding the enthalpies of formation of one or more of the products. These considerations mostly apply to the minor channels that appear only at higher electronic energies, i.e. higher recombination energies of the reactant ion.

All of the reactions measured proceed at the Langevin collision rate and the rate constants are independent of temperature within our relative uncertainty as seen in Tables 1 and 2. Absolute rate constants are difficult to measure at high temperatures because of the low vapor pressure of naphthalene and

the shorter reaction times. Therefore, we report the rate constants for the reaction with N_2^+ and O_2^+ in the HTFA in Table 2 at the two extremes of our temperature range, 630 and 1400 K, which again show no significant temperature dependence.

The atmospheric plasma cations NO^+, O_2^+, O^+, and N^+ undergo nondissociative charge transfer with naphthalene, whereas N_2^+ and ions with higher recombination energies undergo both nondissociative and dissociative charge transfer. Petrie et al. have studied the reactions of Ar^+ and Ne^+ with naphthalene in a SIFT at room temperature [37]. The current results for Ne^+ agree with the previous results to within the experimental error. However, the current Ar^+ results differ significantly from those of Petrie et al. for the branching between the $C_{10}H_8^+$ and $C_{10}H_7^+$ products. Because of this discrepancy, the Ar^+ branching ratios have been thoroughly reexamined. No explanation for this disagreement is apparent. For F^+, some of the reaction also proceeds through the formation of new chemical bonds. Product branching percentages for all of the naphthalene reactions are depicted in Figs. 1–5 plotted against the average total reaction energy in eV neglecting zero point energies. The average reaction energy, $\langle E_{rxn} \rangle$, at flow tube temperature T is thus defined by:

$$\langle E_{rxn} \rangle = RE_{react} + \langle E_{trans} \rangle + \langle E_{rot}^{C_{10}H_8} \rangle + \langle E_{vib}^{C_{10}H_8} \rangle$$
$$+ \langle E_{in}^{ion} \rangle \qquad (1)$$

In the above equation, RE_{react} is the recombination energy of the reactant ion; the average translational energy, $\langle E_{trans} \rangle$, is 3/2 $k_B T$; the average rotational energy in naphthalene, $\langle E_{rot}^{C_{10}H_8} \rangle$, is 3/2 $k_B T$; and the average reactant ion internal energy, $\langle E_{in}^{ion} \rangle$, is $k_B T$ for the diatomic reactant ions. The average naphthalene vibrational energy, $\langle E_{vib}^{C_{10}H_8} \rangle$, is an ensemble average over a Boltzmann distribution of vibrational energy levels for the 48 modes. The average vibrational energies in the O_2^+ and N_2^+ ions at the highest temperatures in the flow tube are negligible, e.g. 0.04 eV at 1400 K. Electronic excitation of the atomic ions is also negligible, i.e. excited states such as the spin-orbit states of Ar^+ are not populated. The average available naphthalene internal energy (rotational

Table 1

Reaction rate constants and product branching percentages for ion–molecule reactions of $C_{10}H_8$ from 300–500 K measured with the VT-SIFT. The collision rate constant, k_c, is given in brackets next to the experimental rate constants. All rate constants are listed in italics and are given in units of 10^{-9} cm^3 s^{-1}. The enthalpies of reaction at 298 K, ΔH_{rxn}, are given in kJ mol^{-1} where the assumed neutral products are given in parentheses. Enthalpies given in braces have been estimated

Reaction (recombination energy, eV)		Rate constant ($\times 10^{-9}$ cm^3 s^{-1}), [k_c] branching ratios				
		ΔH_{rxn}, kJ mol^{-1}	300 K	325 K	370 K	500 K
$NO^+ + C_{10}H_8 \rightarrow$	Products		*1.8* [2.0]		*1.9* [2.0]	
(9.26)	$C_{10}H_8^+ + NO$	-108	1.00		1.00	
$O_2^+ + C_{10}H_8 \rightarrow$	Products		*1.8* [1.9]		*1.8* [1.9]	
(12.07)	$C_{10}H_8^+ + O_2$	-379	1.00		1.00	
$O^+ + C_{10}H_8 \rightarrow$	Products		*2.4* [2.6]		*2.3* [2.6]	
(13.62)	$C_{10}H_8^+ + O$	-529	1.00		1.00	
$N^+ + C_{10}H_8 \rightarrow$	Products		*2.7* [2.7]	*2.9* [2.7]	*2.4* [2.7]	
(14.53)	$C_{10}H_8^+ + N$	-617	1.00	1.00	1.00	
$N_2^+ + C_{10}H_8 \rightarrow$	Products		*2.0* [2.0]	*2.1* [2.0]	*2.0* [2.0]	*2.0* [2.0]
(15.58)	$C_{10}H_8^+ + N_2$	-718	1.00	1.00	1.00	0.94
	$C_8H_6^+ + (C_2H_2) + N_2$	-292				0.04
	$C_6H_6^+ + (C_4H_2) + N_2$	-238				0.02
$Ar^+ + C_{10}H_8 \rightarrow$	Products		*1.7* [1.8]			*1.6* [1.8]
(15.76)	$C_{10}H_8^+ + Ar$	-735	0.95			0.84
	$C_8H_6^+ + (C_2H_2) + Ar$	-310	0.03			0.08
	$C_6H_6^+ + (C_4H_2) + Ar$	-256	0.01			0.04
	$C_5H_5^+ + (C_5H_3) + Ar$	{-38}	0.01			0.04
$F^+ + C_{10}H_8 \rightarrow$	Products		*1.8* [2.4]			
(17.42)	$C_{10}H_7F^+ + H$	-778	0.04			
	$C_{10}H_8^+ + F$	-895	0.15			
	$C_{10}H_7^+ + (HF)$	-1034	0.22			
	$C_{10}H_6^+ + (H_2 + F)$	-453	0.04			
	$C_9H_8^+ + (CF)$	-707	0.01			
	$C_9H_7^+ + (HCF)$	-711	0.01			
	$C_8H_6^+ + (C_2H_2 + F)$	-470	0.28			
	$C_7H_7^+ + (C_3 + HF)$	-498	0.11			
	$C_6H_6^+ + (C_4H_2 + F)$	-416	0.04			
	$C_6H_5^+ + (C_2H_2 + C_2HF)$	{-506}	0.06			
	$C_6H_4^+ + (C_4H_4 + F)$	-132	0.02			
	$C_5H_4^+ + (C_3H_3 + C_2HF)$	-47	0.01			
	$C_5H_3^+ + (C_5H_5 + F)$	-95	0.01			
$Ne^+ + C_{10}H_8 \rightarrow$	Products		*2.3* [2.3]			
(21.56)	$C_{10}H_8^+ + Ne$	-1295	0.04			
	$C_{10}H_7^+ + H + Ne$	-863	0.03			
	$C_{10}H_6^+ + H_2 + Ne$	-853	0.05			
	$C_8H_6^+ + (C_2H_2) + Ne$	-869	0.07			
	$C_8H_5^+ + (C_2H_2 + H) + Ne$	{-575}	0.10			
	$C_7H_5^+ + (C_3H_3) + Ne$	{-738}	0.06			
	$C_7H_4^+ + (C_3H_3 + H) + Ne$	{-474}	0.01			
	$C_6H_6^+ + (C_4H_2) + Ne$	-815	0.04			
	$C_6H_5^+ + (C_2H_2 + C_2H) + Ne$	{-368}	0.23			
	$C_6H_4^+ + (C_4H_4) + Ne$	-532	0.17			
	$C_5H_5^+ + (C_5H_3) + Ne$	{-598}	0.03			
	$C_5H_3^+ + (C_5H_5) + Ne$	-495	0.05			
	$C_4H_4^+ + (C_4H_2 + C_2H_2) + Ne$	-317	0.03			
	$C_4H_2^+ + (3C_2H_2) + Ne$	-125	0.01			
	$C_3H_3^+ + (C_3H_3 + C_4H_2) + C_4H_2$	-269	0.08			

Table 2
Reaction rate constants and product branching ratios for the reaction of N_2^+ and O_2^+ with $C_{10}H_8$ from 500–1400 K measured with the HTFA. The reactant ion recombination energies are also shown. All rate constants are listed in italics and are given in units of 10^{-9} cm^3 s^{-1}. The collision rate constant, k_c, is given in brackets next to the experimental rate constants. The average internal energy (rotational and vibrational energy) in the naphthalene neutral is given for the temperatures used

Reaction (recombination energy)		Rate constant ($\times 10^{-9}$ cm^3 s^{-1}), $[k_c]$ branching ratios				
		500 K	630 K	800 K	1200 K	1400 K
Avg. $C_{10}H_8$ internal energy (eV)		0.47	0.77	1.07	2.46	3.19
$O_2^+ + C_{10}H_8 \rightarrow$ (12.07 eV)	Products		*1.8 [1.9]*		*1.8 [1.9]*	*1.5 [1.9]*
	$C_{10}H_8^+ + O_2$		>0.99		0.97	0.95
	$C_{10}H_7^+ + H + O_2$ } $C_{10}H_6^+ + H_2 + O_2$ }				0.01	0.02
	$C_8H_6^+ + (C_2H_2) + O_2$				0.01	0.02
	$C_9H_n^+$, $C_7H_n^+$, $C_6H_n^+$, $C_5H_n^+$, and $C_4H_n^+$ }				0.01	0.01
$N_2^+ + C_{10}H_8 \rightarrow$ (15.58 eV)	Products	*2.0^a [2.0]*	*1.8 [2.0]*			*1.8 [2.0]*
	$C_{10}H_8^+ + N_2$	0.96	0.84	0.63	0.44	0.28
	$C_{10}H_7^+ + H + N_2$		0.06	0.15	0.23	0.30
	$C_{10}H_6^+ + (H_2) + N_2$			0.02	0.02	0.06
	$C_8H_6^+ + (C_2H_2) + N_2$	0.04	0.08	0.16	0.24	0.27
	$C_8H_5^+ + (C_2H_2 + H) + N_2$					0.01
	$C_6H_6^+ + (C_4H_2) + N_2$		0.01	0.03	0.06	0.06
	$C_6H_5^+ + (C_2H_2 + C_2H) + N_2$					0.01
	$C_9H_n^+$, $C_7H_n^+$, $C_6H_4^+$, $C_6H_3^+$, $C_5H_n^+$, and $C_4H_n^+$ }		0.01	0.01	0.01	0.01

^{a} Value taken from the VT-SIFT. See Table 1.

and vibrational) at the temperatures used in the HTFA is noted in Table 2.

Fig. 1 shows the total percentage of products in each C_n channel measured in the VT-SIFT as a function of total energy. A single symbol represents ions with the same number of carbon atoms but differing numbers of H atoms. Ions with increasingly higher recombination energies provide greater amounts of energy. The branching percentages for the individual $C_{10}H_8^+$, $C_{10}H_7^+$, $C_8H_6^+$, and $C_6H_6^+$ product channels are plotted as a function of total energy in Fig. 2. Breakdown curves for naphthalene have not been published, but breakdown curves are available for the deuterated analogs. Therefore, the relative branching percentages for the deuterated species are also shown in Fig. 2, measured in a T-PEPICO apparatus by Rühl et al. [19], where the photon energy has been varied. The appearance energies of the
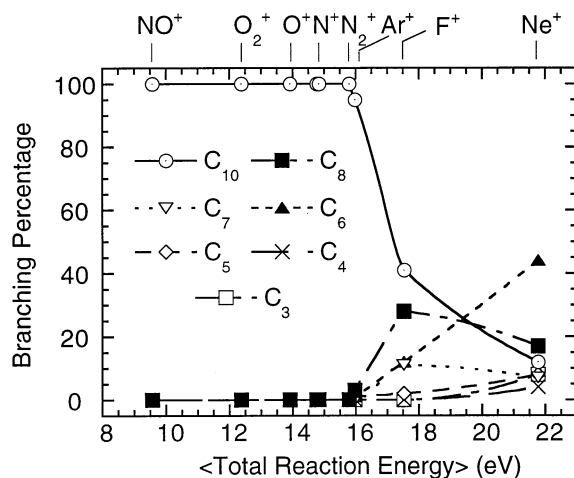
Fig. 1. Branching percentages measured in the VT-SIFT for the various C_n product ion channels plotted as a function of the average total reaction energy in eV at temperatures from 300–370 K. The reaction energy is predominantly electronic energy in the reactant ion as determined by its recombination energy.
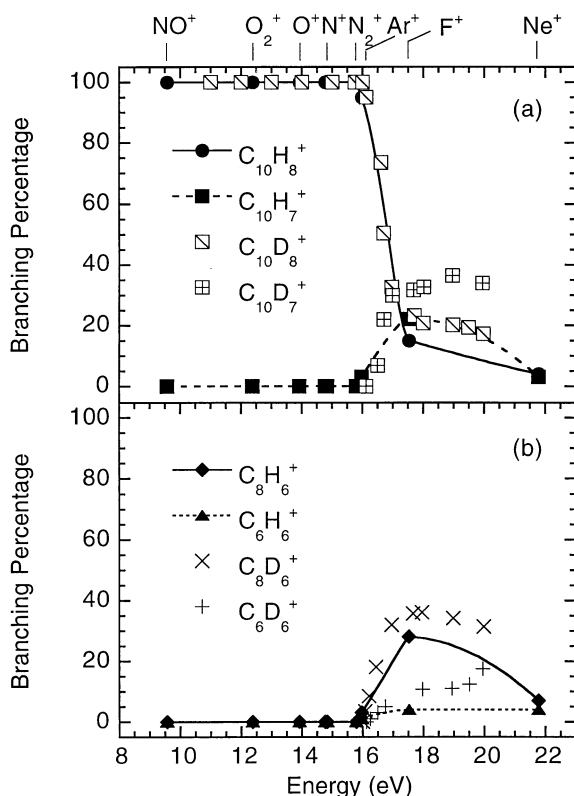
Fig. 2. (a) Branching percentages for $C_{10}H_8^+$, $C_{10}H_7^+$, $C_{10}D_8^+$, and $C_{10}D_7^+$ plotted against the average total reaction energy in eV. (b) Branching percentages for $C_8H_6^+$, $C_6H_6^+$, $C_8D_6^+$, and $C_6D_6^+$ plotted against the average total reaction energy in eV. In both plots, the solid symbols are branching percentages measured at temperatures from 300–370 K in the VT-SIFT, where the reaction energy is predominantly electronic energy in the reactant ion as determined by its recombination energy. The crosses, plus signs, and open symbols are the relative branching percentages for the deuterated product ions taken from breakdown curves measured by Rühl et al. as a function of photon energy using T-PEPICO [19].

deuterated fragment ions are shifted less than 0.2 eV higher than their hydrogenated counterparts [21]. The trends in the branching ratios from the two experiments agree qualitatively. However, the deuterated product branching ratios are higher because Rühl et al. neglect smaller mass channel contributions, as well as corrections for the time-of-flight (TOF) mass spectrometer transmission and hot electron formation. The authors consequently note that the product fractions should be considered "effective" values [19].

Figs. 3–5 show the individual branching percent-
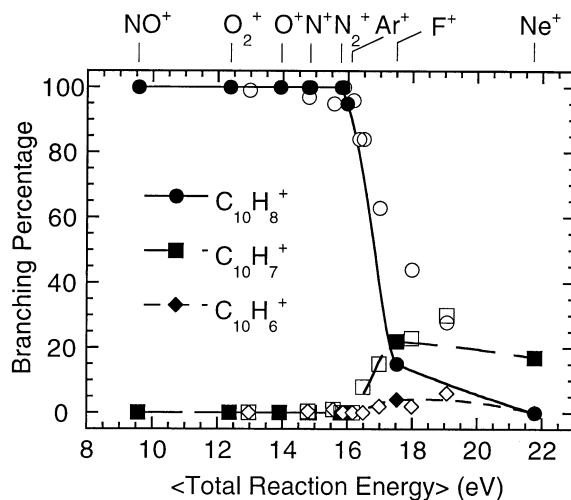
Fig. 3. Branching percentages for the $C_{10}H_m^+$ product channels for $m = 6$–8 plotted vs. the average total reaction energy in eV. The solid symbols reflect primarily electronic excitation in the reactants. The open symbols reflect increasing amounts of internal excitation in vibrational and rotational energy of the reactants measured as a function of temperature from 500–1400 K.

ages for the $C_{10}H_m^+$, $C_8H_m^+$, and $C_6H_m^+$ products plotted versus the average reaction energy given in Eq. (1). The solid symbols represent 300 K data where
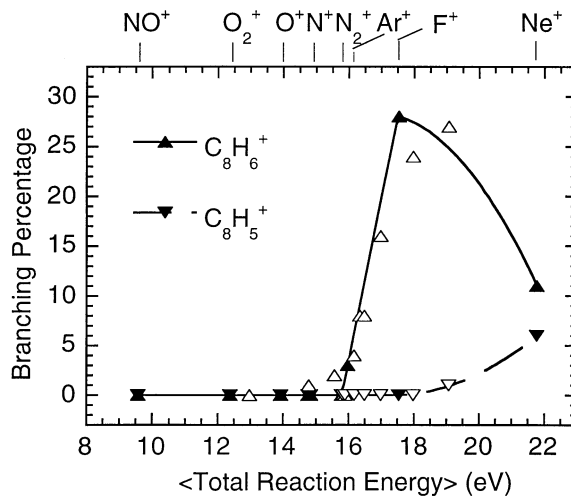
Fig. 4. Branching percentages for the $C_8H_m^+$ for $m = 5$–6 plotted vs. the average total reaction energy in eV. The solid symbols reflect primarily electronic excitation in the reactants. The open symbols reflect increasing amounts of internal excitation in vibrational and rotational energy of the reactants measured as a function of temperature from 500–1400 K.
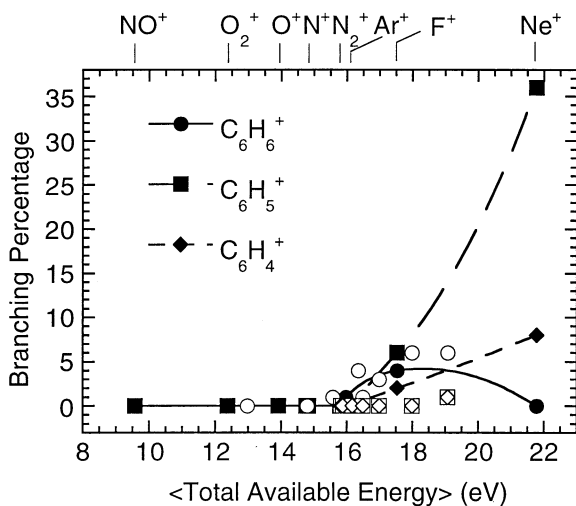
Fig. 5. Branching percentages for the $C_6H_m^+$ for $m = 4$–6 plotted vs. the average total reaction energy in eV. The solid symbols reflect primarily electronic excitation in the reactants. The open symbols reflect increasing amounts of internal excitation in vibrational and rotational energy of the reactants measured as a function of temperature from 500–1400 K.

the total energy is varied by changing the recombination energy of the ion. The open symbols reflect an increasingly larger fraction of the available energy coming from internal excitation of the naphthalene as the temperature is raised.

3.1. $C_{10}H_m^+$ products

The branching percentages of the charge transfer product $C_{10}H_8^+$ and the two hydrogen loss products $C_{10}H_7^+$ and $C_{10}H_6^+$ are plotted versus the average total reaction energy in Fig. 3. The solid symbols represent the branching percentages measured at 300 K in the VT-SIFT, and the line is interpolated to fit the points. For these data, increasing the energy reflects an increase in the recombination energy of the reactant ion. For comparison, the open symbols give the percentages measured at temperatures above 300 K. In this case a larger portion of the reaction energy is neutral reactant internal energy—over 3 eV for a temperature of 1400 K. Both hydrogen loss products have a common onset, as seen previously in photo-

ionization mass spectrometry (PIMS) experiments [20].

High temperature data from the O_2^+ reaction show an onset of $C_{10}H_8^+$ dissociation slightly lower than the other data sets. This may arise from pyrolysis of the naphthalene reagent in the flow tube. However, the amount of fragmentation totals 5%, indicating that 5% or less degradation occurs at high temperatures. The lack of significant decomposition at 1400 K is consistent with the fact that aromatic species are stable products of hydrocarbon pyrolysis [1]. Alternatively, the slightly different onset may reflect a broader energy distribution at high temperature. Changing the recombination energy does not affect the energy spread in the reactivity at 300 K because the ionization potentials are well defined. However, elevating the temperature not only increases the energy, but also broadens the distribution appreciably because thermal distribution functions define the average vibrational and rotational energies.

As the energy increases, the amount of nondissociative charge transfer products decreases with a concomitant increase in the fraction of dissociative charge transfer products, i.e. the hydrogen loss products. This trend is not surprising because the fragmentation channels are highly exothermic, as seen in Table 1. If the effect of internal energy (open symbols) versus electronic energy (solid symbols) is compared, differences between the high temperature N_2^+ data and the F^+ data become apparent. However, reactive channels that produce HF cannot be ruled out, as will be discussed later. The same comparison shows no effect for $C_{10}H_7^+$ and $C_{10}H_6^+$ formation.

3.2. $C_8H_m^+$ products

The branching percentages for $C_8H_6^+$ and $C_8H_5^+$ are plotted relative to the average reaction energy in Fig. 4. Increasing the recombination energy increases the amount of $C_8H_6^+$ observed compared to increasing the internal energy. This is one of several channels that offsets the difference in the $C_{10}H_8^+$ product with the different types of energy just described. Increasing energy yields a greater amount of $C_8H_5^+$ and both types of energy appear to be equally effective in

driving this channel. The onset for this channel is higher than the channels previously discussed, including $C_8H_6^+$.

3.3. $C_6H_m^+$ products

The branching percentages for $C_6H_6^+$, $C_6H_5^+$, and $C_6H_4^+$ plotted against the average total reaction energy are illustrated in Fig. 5. As with the other major products, $C_6H_6^+$ has an energetic threshold of ~16 eV. If the extrapolation to the baseline through the VT-SIFT data (solid symbols) is used to estimate the onset of $C_6H_5^+$ and $C_6H_4^+$, the products also appear at ~16 eV. The temperature-dependent data have an onset above 18 eV for these two channels. This may be a real effect or may reflect the fact that the 300 K point at 17.42 eV represents the reaction of F^+ with naphthalene, for which hydride anion abstraction giving HF is highly exothermic. Thus, the branching percentages for the $C_6H_5^+$ and $C_6H_4^+$ channels may be higher if HF formation occurs. A threshold closer to 18 eV is consistent with the PIMS results where no reactive channels interfere [20].

4. Discussion

Experimental appearance energies reflect the time-scale of observation in the particular apparatus. When ions dissociate slowly, they may not have time to fragment before being detected. Therefore, the required energy for dissociation appears higher than the actual threshold value, producing a kinetic shift [38]. The time-dependent photodissociation results of Lifshitz and co-workers have been fit using RRKM rate constants for the unimolecular decay of $C_{10}H_8^+$. The C–H bond dissociation energy of 4.48 eV (432 kJ mol^{-1}) obtained [24] intimates an appearance potential of 12.62 eV. The ~16 eV appearance potential observed in the flow tube experiments and the PIMS measurements [20] differs significantly from the appearance energy derived from the C–H bond dissociation energy. This value is over 3 eV greater than the thermochemical value, indicating that a large kinetic shift occurs [22,24]. The energetics of acetylene loss

from $C_{10}H_8^+$ have also been well established by time-dependent measurements and RRKM theory to require 4.41 eV [24], corresponding to an appearance energy of 12.55 eV. This value implies a similar 3 eV kinetic shift as observed with $C_{10}H_7^+$. The appearance potentials are based on the observation that simple bond fissions do not usually have activation barriers beyond the reaction endothermicity.

The earlier PIMS experiments [14,20] can detect fragments formed at a unimolecular dissociation rate of around 10^4 s^{-1}. Using plots of the unimolecular dissociation rate as a function of internal energy from Ho et al. [24], the naphthalene cation internal energy required for this dissociation rate is 7.5 eV, giving an appearance energy of around 15.5 eV (exactly as Jochims et al. observe [14,20]). These rate-energy curves reveal that the naphthalene cation has an extraordinarily long lifetime. Our observation time is around 1 ms, so that the threshold for dissociation on this timescale taken from the aforementioned curve should be around 15 eV. However, our observed threshold is ~16 eV, about 1 eV higher.

The major difference between the two sets of experiments is the operating pressure. The PIMS experiments of Jochims et al. [14,20] have been conducted at pressures under 10^{-4} Torr [39], whereas the flow tube measurements are taken at 0.5–1 Torr. Eq. (2) gives a simple kinetic model for the fraction of $C_{10}H_8^+$ detected relative to the amount of excited $C_{10}H_8^+*$ initially formed. The equation includes a collisional quenching term that accounts for collisional stabilization of $C_{10}H_8^+*$ in competition with unimolecular dissociation and radiative relaxation

$$[C_{10}H_8^+]_{\tau_x}/[C_{10}H_8^+*]_0$$

$$= e^{-(k_{uni}+k_{rad}+k_Q[M])\tau_x} + \frac{k_{rad}+k_Q[M]}{k_{uni}+k_{rad}+k_Q[M]}$$

$$\times (1 - e^{-(k_{uni}+k_{rad}+k_Q[M])\tau_x}) \qquad (2)$$

The rates of unimolecular dissociation, collisional quenching, and radiative decay are given by k_{uni}, $k_Q[M]$, and k_{rad}, respectively, in s^{-1} and the reaction time τ_x at a given flow tube position x is in seconds. $[M]$ represents the number density of helium atoms in

the flow tube. The radiative relaxation rate for naphthalene cation is ~ 1 s^{-1} [40,41]. Collisional stabilization of the energized $C_{10}H_8^{+}$* is a consequence of the approximately 10^{16} cm^{-3} number density of He buffer gas present under typical flow tube conditions, where τ_x is 1 ms on average. According to Eq. (2), $k_{uni} \cong k_Q[M]$ at the 50% point of the $C_{10}H_8^{+}$ breakdown curve. This point occurs at a reaction energy of about 16.8 eV, allowing k_{uni} to be obtained from the rate-energy curves of Ho et al. [24]. Substituting k_{uni} and $[M]$ into the equality mentioned gives k_Q of $\sim 0.5 \times 10^{-10}$ cm^3 s^{-1}. Considering the Langevin collision rate between He and $C_{10}H_8^{+}$* of 5.38×10^{-10} cm^3 s^{-1}, the k_Q value derived implies that ~ 10 collisions with the buffer gas are required for stabilizing $C_{10}H_8^{+}$* for a period longer than 1 ms. This result is consistent with work done on ion–molecule association reactions that also indicates that numerous helium collisions are necessary to stabilize complexes [42]. Therefore, a kinetic shift, coupled with collisional quenching by the helium buffer gas, accounts for the differences between the experimental and thermochemical dissociation energies. The long lifetime of the nascent $C_{10}H_8^{+}$ ion facilitates the large shifts observed.

In spite of these complications, we can speculate about the mechanism for $C_{10}H_8^{+}$ dissociation. Because the qualitative trends in our results and the PIMS results of Jochims et al. [20] agree, we adopt their mechanism for $C_{10}H_8^{+}$ dissociation. The electron impact ionization [16] and PIMS measurements show common dissociation thresholds for the $C_{10}H_7^{+}$, $C_{10}H_6^{+}$, $C_8H_6^{+}$, and $C_6H_6^{+}$ product ions observed at lower appearance energies [16]. Jochims et al. also observe a common dissociation threshold for the lower energy products. Consequently, Jochims et al. conclude that the $C_{10}H_8^{+}$ ions originate from a common naphthalene-like cationic intermediate [20]. The thresholds for $C_{10}H_7^{+}$ and $C_8H_6^{+}$ established by an RRKM theory fit to time-dependent photodissociation data also confirm that these products have a common threshold independent of kinetic shifts [22,24]. On the contrary, recent photodissociation experiments indicate that naphthalene cations fragment by sequential C_2H_2 loss in contrast to the common intermediate

hypothesis discussed above. However, the authors of the photodissociation studies acknowledge that they are probably not observing the lowest energy dissociation channels because the broadband light source used is uncharacterized [28].

Above 18.5 eV, the bicyclic cation intermediate may isomerize into an open chain isomer that dissociates into smaller open chain products with higher appearance energies [20]. Therefore, the minor product channels we observe are assumed to have an open chain configuration in calculating reaction enthalpies, yielding similar neutral products to those postulated by Jochims et al. [20]. Because of the substantial shifts in the experimental appearance energies just discussed, these values make it difficult to identify the reaction products.

4.1. $C_{10}H_m^{+}$ products

The common appearance energy onset, along with the energetics of H atom removal from $C_{10}H_7^{+}$, precludes the formation of $C_{10}H_6^{+}$ from decomposition of $C_{10}H_7^{+}$, where sequential H atom loss would require 1 eV of energy above the observed threshold. Kinetic shifts should also make the apparent onset even higher in energy. Consequently, both hydrogen loss channels probably arise from the $C_{10}H_8^{+}$ intermediate [20]. We observe this threshold at around 16 eV, close to the value of Jochims et al. [20].

4.2. $C_8H_m^{+}$ products

The $C_8H_6^{+}$ products are assumed to come from acetylene loss in $C_{10}H_8^{+}$ to generate the phenylacetylene isomer [20], because it is the lowest energy structure [34]. However, recent ab initio calculations [26] suggest that the bicyclic benzocyclobutadiene isomer may be ~ 0.1 eV more stable. The authors note that this difference is within the error of the calculations so that the two may be equally stable [26]. Nevertheless, we have assumed that the product ion has the phenylacetylene structure for calculating enthalpies of reaction. As already mentioned, the $C_8H_5^{+}$ is assumed to arise from a linear precursor; in this case, olefinic hydrogen loss from an open chain $C_8H_6^{+}$

isomer formed at high energy [20]. This is consistent with the higher onset energy.

The $C_8H_6^+$ channel has an observed threshold around 15.8 eV. Extrapolating the line through the $C_8H_5^+$ data to the baseline in Fig. 4 yields an experimental onset of about 18.5 eV. This threshold is consistent with removing an H atom from a higher energy open chain isomer [20]. However, the loss of an H from the acetylene substituent of phenylacetylene is energetically possible and cannot be ruled out as a possible mechanism at the highest reaction energies [20] where almost 10 eV excess energy is accessible. Loss of a hydrogen atom from either ring of the cyclobutadiene $C_8H_6^+$ isomer is exothermic as well.

4.3. $C_6H_n^+$ products

Acknowledging that the appearance energies may have as much as 3 eV kinetic shift, the only energetically possible structures for $C_6H_6^+$ can be either the benzene or fulvene cations [19]. However, the benzene cation is the most likely form considering that it requires only two hydrogen shifts and two C–C bond cleavages in a naphthalene cation intermediate. The common threshold of $C_6H_6^+$ and the other major products believed to arise from a single intermediate of this type supports this assertion [20]. In addition, generating the fulvene cation necessitates an additional isomerization, which is a more complicated mechanism. Nevertheless, the $C_6H_5^+$ and $C_6H_4^+$ structures are not readily apparent based simply on energetics. It is not possible to distinguish whether open chain structures form or a benzene cation loses hydrogen atoms based solely on the appearance energies, especially considering that kinetic shifts occur [20]. Both mechanisms are thus feasible at the energies where the products appear.

4.4. High energy product channels

The products that arise only in the reactions with F^+ and Ne^+ are referred to as the high-energy products because over 9 eV of excess energy can be put into the nascent $C_{10}H_8^+$. The excessive energy affords substantial ring fragmentation. Jochims et al. have proposed that the $C_{10}H_8^+$ intermediate with its transannular ring bond broken can use the extra energy to form an open chain $C_{10}H_8^+$. This linear species can be dissected into smaller fragments, producing the ions observed with appearance energies above 18 eV [20]. However, the benzene cation can also dissociate through competing pathways [43–46], some of which yield similar C_3–C_5 products [47]. We have also observed these products in recent flow tube experiments of ion–molecule reactions of benzene [9]. All of the $C_5H_m^+$ and smaller ionic fragments are energetically accessible from either a linear precursor or from the benzene cation with Ne^+ as the reactant ion.

In addition, recombination of the neutral products with F makes several of the fragmentation reactions exothermic, and both a cyclic and a linear mechanism are possible in the F^+ reactions as well. F^+ can abstract a hydride anion to form HF in a very exothermic reaction. Another recent study of dissociative charge transfer involving halide-containing molecules has shown evidence for HF and HCl formation [48]. Other chemical pathways involving CF bond formation are also possible, and, in fact, a minor channel forming $C_{10}H_7F^+$ has been observed. Again, the large kinetic shifts in the experimental appearance energies preclude the elimination of a specific pathway simply based on thermochemistry. As a result, we cannot differentiate whether the dissociation products observed at high energies form via cyclic or linear intermediates.

5. Conclusions

Temperature dependent rate constants and product branching ratios have been measured for the reactions of naphthalene with the atmospheric plasma ions NO^+, N_2^+, N^+, O^+, and O_2^+, as well as several higher energy ions, Ar^+, F^+, and Ne^+ in a VT-SIFT. In the case of N_2^+ and O_2^+, the reactions have been studied over an extended temperature range from 300–1400 K. Branching ratios have been measured for the first time in the high temperature flowing afterglow, ex-

panding the capabilities of this apparatus. All of the reactions proceed at the Langevin collision rate, yielding nondissociative and dissociative charge transfer products. The fraction of dissociation products increases as the average reaction energy increases. The results further demonstrate that using reactant ions with successively higher recombination energies gives breakdown curves similar to photodissociation measurements at different photon energies. In addition, the reaction with F^+ may partially proceed by chemical reaction. The onsets of the dissociative channels exceed the thermodynamic thresholds due to both kinetic shifts and collisional quenching of the nascent excited species by the helium buffer gas.

One of the goals of the present study was to search for the effects of internal energy of the reactants on the dissociation rate. Comparing the energy added through temperature (open symbols) to the energy added through ion recombination energy (closed symbols) shows that for many of the product channels little difference is found, i.e. for the $C_{10}H_7^+$, $C_{10}H_6^+$, $C_8H_5^+$, and $C_6H_6^+$ channels. In other cases, differences are observed, such as for $C_{10}H_8^+$, $C_6H_5^+$, and $C_6H_4^+$.

It is possible to store large amounts of vibrational energy in naphthalene because of the 48 vibrational degrees of freedom available, many of them being low or moderate frequency [49]. At 800, 1100, and 1400 K, approximately 1, 2, and 3 eV of vibrational energy is stored in naphthalene. The energy spread is also large when energy is added through temperature. For the parent ion, $C_{10}H_8^+$, the dissociation threshold seems to shift slightly to lower energy for the O_2^+ data at high temperature, compared to the N_2^+ and Ar^+ 300 K data. As explained previously, the energy spread in the high temperature experiments or a small amount of dissociation of naphthalene may account for this shift. The higher temperature data for the N_2^+ reactions show more of the nondissociative charge transfer channel than the 300 K point with F^+ (17.5 eV). The extra fragmentation with F^+ is found in the $C_8H_6^+$, $C_6H_5^+$, $C_6H_4^+$, and some of the smaller fragments. Most of the ions in this study are either ions formed in air discharges or are nonreactive so that nondissociative and dissociative charge transfer com-

pletely govern the reactivity. Unfortunately, at energies above 16 eV few such ions exist; therefore F^+ is the simplest, most logical choice. This makes the above comparisons difficult to interpret because reactive channels may interfere. Thus, the differences found when looking for specific types of energy effects when F^+ is involved can be due to several factors: (1) energy spread, (2) reactive pathways, or (3) the type of energy. Because many of the channels behave similarly, it appears that much of the reactivity is independent of all three of these effects. The chemistry of this large molecule is very complex and we cannot speculate further on how different types of energy affect the dissociation based on our current results.

The strong kinetic shifts observed have implications for models of carbon growth reactions in combustion systems. Over 3 eV of internal energy above the thermochemical threshold must be added for the unimolecular decay rate of $C_{10}H_8^+$ to be observable on our experimental timescale. Larger PAH molecules will exacerbate the situation because the ion lifetimes increase with increasing size. Consequently, higher internal energies are required for fragmentation on short timescales [14]. Any theoretical predictions that include ionic PAH constituents must therefore account for the long dissociation lifetimes, as well as the pressure effects on the branching ratios introduced by collisional stabilization.

Acknowledgements

References

[1] D.L. Trimm, in Pyrolysis: Theory and Industrial Practice, L.F. Albright, B.L. Crynes, W.H. Corcoran (Eds.), Academic, New York, 1983, p. 203.

[2] L.Q. Maurice, T. Edwards, R.C. Striebich, Proceedings of the AIAA/ASME/SAE/ASEE 34th Joint Propulsion Conference, Cleveland, July 1998, AIAA 98-3534.

[3] P. Gerhardt, K.-H. Homann, J. Phys. Chem. 94 (1990) 5381.

[4] P. Weilmunster, A. Keller, K.-H. Homann, Combust. Flame 116 (1999) 62.

[5] S.T. Arnold, A.A. Viggiano, R.A. Morris, J. Phys. Chem. A 101 (1997) 9351.

[6] S.T. Arnold, R.A. Morris, A.A. Viggiano, J. Phys. Chem. A 102 (1998) 1345.

[7] S.T. Arnold, A.A. Viggiano, R.A. Morris, J. Phys. Chem. A 102 (1998) 8881.

[8] S. Williams, S.T. Arnold, P.M. Bench, A.A. Viggiano, I. Dotan, A.J. Midey, T. Morris, R.A. Morris, L.Q. Maurice, E.A. Sutton, Proceedings of the 14th International Symposium on Air Breathing Engines, Florence, September 1999, ISABE 99-7236.

[9] S.T. Arnold, S. Williams, I. Dotan, A.J. Midey, R.A. Morris, A.A. Viggiano, J. Phys. Chem. A 103 (1999) 8421.

[10] D.K. Bohme, Chem. Rev. 92 (1992) 1487.

[11] A. Leger, J.L. Puget, Astron. Astrophys. 137 (1984) L5.

[12] L.J. Allamandola, A.G.G.M. Tielens, J.R. Barker, Astrophys. J. 290 (1985) L25.

[13] L.J. Allamandola, D.M. Hudgins, S.A. Sandford, Astrophys. J. 511 (1999) L115.

[14] H.W. Jochims, E. Ruhl, H. Baumgartel, S. Tobita, S. Leach, Astrophys. J. 420 (1994) 307.

[15] H.W. Jochims, H. Baumgartel, S. Leach, Astrophys. J. 512 (1999) 500.

[16] R.J. van Brunt, M.E. Wacks, J. Chem. Phys. 41 (1964) 3195.

[17] M.S. Kim, R.C. Dunbar, J. Chem. Phys. 72 (1980) 4405.

[18] J.A. Syage, J.E. Wessel, J. Chem. Phys. 87 (1987) 3313.

[19] E. Ruhl, S.D. Price, S. Leach, J. Phys. Chem. 93 (1989) 6312.

[20] H.W. Jochims, H. Rasekh, E. Ruhl, H. Baumgartel, S. Leach, Chem. Phys. 168 (1992) 159.

[21] H.W. Jochims, H. Rasekh, E. Ruhl, H. Baumgartel, S. Leach, J. Phys. Chem. 97 (1993) 1312.

[22] Y. Gotkis, M. Oleinikova, M. Naor, C. Lifshitz, J. Phys. Chem. 97 (1993) 12 282.

[23] H. Abouelaziz, J.C. Gomet, D. Pasquerault, B.R. Rowe, J.B.A. Mitchell, J. Chem. Phys. 99 (1993) 237.

[24] Y.P. Ho, R.C. Dunbar, C. Lifshitz, J. Am. Chem. Soc. 117 (1995) 6504.

[25] M.J. DeWitt, R.J. Levis, J. Chem. Phys. 102 (1995) 8670.

[26] G. Granucci, Y. Ellinger, P. Boissel, Chem. Phys. 191 (1995) 165.

[27] X. Wang, H. Becker, A.C. Hopkinson, R.E. March, L.T. Scott, D.K. Bohme, Int. J. Mass Spectrom. Ion Processes 161 (1997) 69.

[28] S.P. Ekern, A.G. Marshall, J. Szczepanski, M. Vala, J. Phys. Chem. A 102 (1998) 3498.

[29] A.A. Viggiano, R.A. Morris, F. Dale, J.F. Paulson, K. Giles, D. Smith, T. Su, J. Chem. Phys. 93 (1990) 1149.

[30] P.M. Hierl, J.F. Friedman, T.M. Miller, I. Dotan, M. Mendendez-Barreto, J. Seeley, J.S. Williamson, F. Dale, P.L. Mundis, R.A. Morris, J.F. Paulson, A.A. Viggiano, Rev. Sci. Instrum. 67 (1996) 2142.

[31] D.R. Lide (Ed.), CRC Handbook of Chemistry and Physics, CRC, Boca Raton, 1996, p. 6.

[32] A.A. Viggiano, R.A. Perry, D.L. Albritton, E.E. Ferguson, F.C. Fehsenfeld, J. Geophys. Res. 85 (1980) 4551.

[33] C. Praxmarer, A. Hansel, W. Lindinger, Z. Herman, J. Chem. Phys. 109 (1998) 4246.

[34] S.G. Lias, J.E. Bartmess, J.F. Liebman, J.L. Holmes, R.D. Levin, W.G. Mallard, in NIST Chemistry WebBook, NIST Standard Reference Database Number 69, W.G. Mallard, P.J. Linstrom (Eds.), NIST, Gaithersburg, 1998 (http://webbook.nist.gov).

[35] K. Lammertsma, P.v.R. Schleyer, J. Am. Chem. Soc. 105 (1983) 1049.

[36] V.L. Page, Y. Keheyan, V.M. Bierbaum, T.P. Snow, J. Am. Chem. Soc. 119 (1997) 8373.

[37] S. Petrie, G. Javahery, A. Fox, D.K. Bohme, J. Phys. Chem. 97 (1993) 5607.

[38] S.G. Lias, J.E. Bartmess, J.F. Liebman, J.L. Holmes, R.D. Levin, W.G. Mallard, J. Phys. Chem. Ref. Data 17 (Suppl. 1) (1988) 1.

[39] K. Rademann, H.W. Jochims, H. Baumgartel, J. Phys. Chem. 89 (1985) 3459.

[40] R.C. Dunbar, J.H. Chen, H.Y. So, J. Chem. Phys. 86 (1987) 2081.

[41] Y.-P. Ho, Y.-C. Yang, S.J. Klippenstein, R.C. Dunbar, J. Phys. Chem. 99 (1995) 12 115.

[42] Y. Ikezoe, S. Matsuoka, M. Takebe, A.A. Viggiano, Gas Phase Ion-Molecule Reaction Rate Constants Through 1986, Maruzen, Tokyo, 1987.

[43] T. Baer, G.D. Willett, D. Smith, J.S. Phillips, J. Chem. Phys. 70 (1979) 4076.

[44] M.F. Jarrold, W. Wagner-Redeker, A.J. Illies, N.J. Kirchner, M.T. Bowers, Int. J. Mass Spectrom. Ion Processes 58 (1984) 63.

[45] H. Kuhlewind, A. Kiermeier, H.J. Neusser, J. Chem. Phys. 85 (1986) 4427.

[46] S.J. Klippenstein, J.D. Faulk, R.C. Dunbar, J. Chem. Phys. 98 (1993) 243.

[47] R. Chawla, A. Shukla, J. Futrell, Int. J. Mass Spectrom. Ion Processes 165/166 (1997) 237.

[48] T.L. Williams, L.M. Babcock, N.G. Adams, Int. J. Mass Spectrom. 185/186/187 (1999) 759.

[49] F.M. Behlen, D.B. McDonald, V. Sethuraman, S.A. Rice, J. Chem. Phys. 75 (1981) 5685.